Central European Journal of Energetic Materials
ISSN 1733-7178; e-ISSN 2353-1843


*Cent. Eur. J. Energ. Mater.* 2022, *19*(4): 409-423; DOI 10.22211/cejem/158316
Article is available in PDF-format, in colour, at:
https://ipo.lukasiewicz.gov.pl/wydawnictwa/cejem-woluminy/vol-19-no-4/?lang=en


***Research paper***

# Anisotropic Interfacial Adhesion between Fluoropolymers and RDX Single Crystal Faces

**Jiahui Liu*), Xiaoqing Zhou, Wen Qian, Feiyan Gong, Zhijian Yang, Hongzheng Li, Fude Nie**
*Institute of Chemical Materials, China Academy of Engineering Physics, Mianyang , 621900, China*
**E-mail:* huiihuii@163.com

**Abstract:** Interfacial interactions have an important influence on the properties of energetic materials. The anisotropy of interfacial adhesive strength between various 1,3,5-trinitro-1,3,5-triazinane (RDX) single crystal faces and a typical binder was studied in this work by experimental and theoretical investigations. An RDX single crystal was prepared and processed into three kinds of orientated crystal faces, including (002), (020) and (210). These crystal slices were used as substrates, and fluorinated polymer F2314 was used as a binder. The surfaces of the RDX slices were analyzed by X-ray photoelectron spectroscopy (XPS) and an atomic force microscope (AFM). The work of adhesion was obtained from direct tensile tests, using designed samples of the sandwich structure of RDX-F2314-RDX, with various RDX single crystal surfaces. The polarity component of the surface energy and the work of adhesion was obtained by Young's equation and the Fowkes theory, based on surface contact angle tests. The results in this work indicated the anisotropy of the interfacial adhesion of F2314 on various RDX crystal faces.

**Keywords:** energetic materials, interfacial adhesive strength, anisotropy, RDX, single crystal

## Supplementary Information (SI)

In the SI are presented some data taken from a national standard of China GB-T5210-2006 Colour paint and varnish method adhesion test.

## 1 Introduction

Polymer bonded explosives (PBXs) are functional composite materials composed of explosive crystals and polymer binders [1-4]. The performances of PBXs are mainly determined by the state of the explosive particles, the binder and the interfacial interaction between them [5-8]. Debonding at the interface will undoubtedly lead to performance deterioration of a PBX [9, 10]. Therefore, the study of the interfacial interaction between an explosive crystal and a binder has been a hot issue in the current field of energetic materials [11-15].

The anti-debonding ability of PBXs is directly determined by the interfacial adhesion strength between the energetic crystals and the polymer binders. The interfacial adhesive strength is commonly obtained based on the surface energy of materials, which can be indirectly calculated according to Young's equation and the Fowkes equation. For example, when the surface energy of 1,3,5-triamino-2,4,6-trinitrobenzene (TATB) and 1,3,5,7-tetranitro-1,3,5,7-tetrazocane (HMX) is obtained by the Zisman technique, the interfacial force between TATB, HMX and fluoropolymers may be calculated [16]. Du Meina used the thin layer capillary permeation technique (Washburn method) to obtain the surface energy of 1,3,5-trinitro-1,3,5-triazinane (RDX) and studied the effect of the interfacial adhesive strength on the mechanical properties of propellants with RDX/HTPB [17]. Although the data obtained from the contact angle test are horizontally comparable, these methods still have some limitations. For instance, the contact angle results would be unstable if the tested liquid flows into the pores, which is inevitable on the tablet during the test. In addition, since most of the explosive crystals exhibit anisotropic performance due to different molecular arrangements [18-20], anisotropic interfacial adhesion may exist between the binder and different crystal faces. A weak interface might cause vulnerability, which will be unfavorable for the performances of the PBX.

Therefore, the understanding of the structure-properties relationships in PBXs will be improved, for instance in providing guidance for tuning the predominant crystal faces, if the interfacial adhesion between different explosive crystal faces and binders can be effectively measured. To the best of our knowledge, directly measuring the adhesive strength between energetic crystals and binders by experimental means has been rarely reported. Williamson *et al.* [21] jointed two large HMX particles with a binder, and then stretched them using a material testing machine. The stress-strain curve was recorded when the binder became detached from the HMX. This method was straight forward in testing the interaction of the explosive crystals with the binder. However, any anisotropic interfacial adhesion was not considered in the literature.

Taking the voids and anisotropy into account, the integrate crystal should be an ideal material to investigate the interfacial interaction. However, the common size of an explosive crystal is about several to a few hundred microns in scale, which is not suitable for such experiments. With the support of the preparation technology for large single crystals [22], numerous pores between small crystals can be avoided. Besides, single crystal slices with different orientations can be obtained by directional cutting techniques [23], which is helpful for studying the anisotropy of the surface energy and interfacial interaction between crystal and binder. In the present paper, various RDX single crystal slices were used as substrates, and fluoropolymer F2314 was used as the binder film. The surface energy of three different RDX crystal faces were calculated *via* thermodynamic equations, and the interfacial interaction between RDX and F2314 was measured directly by tensile experiments. The anisotropic interfacial adhesion between fluoropolymer F2314 and different RDX single crystal faces was compared by various methods and is discussed.

## 2 Experiment

### 2.1 Materials

RDX was prepared by the Institute of Chemical Materials, CAEP of China. F2314 (a copolymer of vinylidene fluoride and chlorotrifluoroethylene in the ratio 1:4) was used as the polymer binder and was provided by Zhonghao Chenguang Chemical Industry Co., Ltd. China. Acetone, ethyl acetate and di-iodomethane were purchased from Sigma-Aldrich Co., Ltd.

### 2.2 Preparation of RDX crystal slices with different orientations

Firstly, the RDX powder was dissolved in acetone at room temperature to obtain a saturated solution, which was filtered through a 0.22 μm microporous membrane filter, and the filtrate was placed in a constant temperature incubator at 30 °C. The solvent was slowly evaporated to obtain a large single crystal. A low-speed diamond wire cutter was used to cut along the parallel direction of a single crystal face under cooling water to obtain RDX slices with different crystal orientations. In order to avoid the influence of surface roughness on the interface adhesion in the contact angle test, a glass turntable was used to polish the RDX slices, and then felt was used to polish precisely.

## 2.3 Characterizations

The contact angle of the liquid on the F2314 film and the different RDX orientation slices was measured using an SL200B contact angle meter. Water and di-iodomethane were selected as test liquids. The droplet diameter of the test solution was controlled to be 1-2 mm. Each contact angle was measured at least three times and the average value was calculated as the adopted data.

The surface elements of various RDX crystal faces after being coated with F2314 binder was characterized by using X-ray photoelectron spectroscopy (XPS; ThermoFisher spectrometer) equipped with monochromatic Al Ka radiation (1486.6 eV). All of the XPS measurements were done with a spot size of 400 μm.

The surfaces of various RDX crystal faces were characterized by using an atomic force microscope (AFM; SPA-300HV, Seiko Instruments) with an SPI 3800 N controller. Etched silicon tips, with a resonance frequency of 70 kHz and a force rate of 42 N/m, were used for the scans.

Samples for the XRD, XPS and AFM characterizations: the RDX slices were coated with F2314 binder using a rinsing method. Briefly, F2314 binder solution of 4% concentration was prepared for use;RDX slices were then soaked in the solution and taken out after 1 min; RDX slices with uniform F2314 binder were obtained after being dried in air for 24h. The samples were characterized by XRD, XPS and AFM. Naked RDX crystal slices were tested for reference.

**(a)**

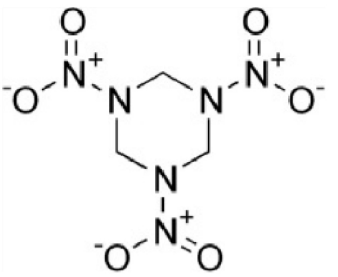

**(b)**

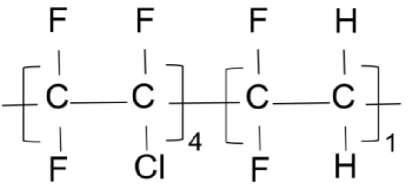

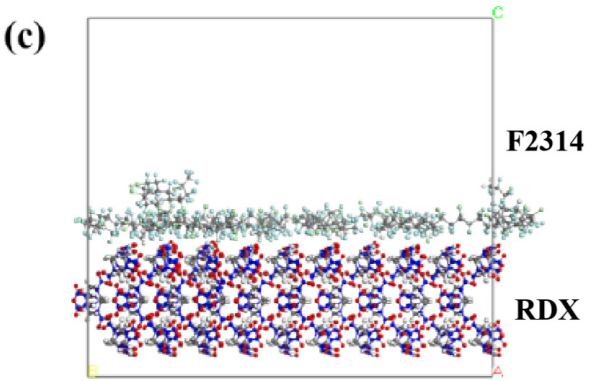


**Figure 1.** RDX molecular formula (a), F2314 polymer repeat unit (b) and interfacial molecular model F2314-RDX(002) (c)

## 2.6 Measurement of adhesive strength

The adhesive strength between an RDX slice and the F2314 binder was measured by a tensile test, which involved the pull-out method as described in GB-T5210 [24] (see Supporting Information). Samples for the tensile test are schematically presented in Figure 2(a) and were prepared as follows: firstly, the RDX slice (named RDX slice A and RDX slice B, with the same orientation and area) was bonded to an aluminum pedestal (named pedestal A and pedestal B, respectively) using a strong glue, as shown in Figure 2(a); secondly, both RDX slices, A and B, were coated with 0.05 g of 12 wt.% F2314 solution in ethyl acetate; thirdly, RDX slice A and RDX slice B were bonded by the F2314 binder into a sandwich-like structure of RDX-F2314-RDX, as shown in Figure 2(c); finally, the sample was used for the tensile test after 24 h, when the solvent (ethyl acetate) had fully volatilized. During the tensile test, the clips of pedestal A and pedestal B were fixed to the stretching clamps of the material testing machine (Figure 2(d) and Figure 2(e)). The tensile rate was 0.6 mm/min. The stress-displacement curve was recorded until interface debonding occurred, which was used to calculate the adhesive work.

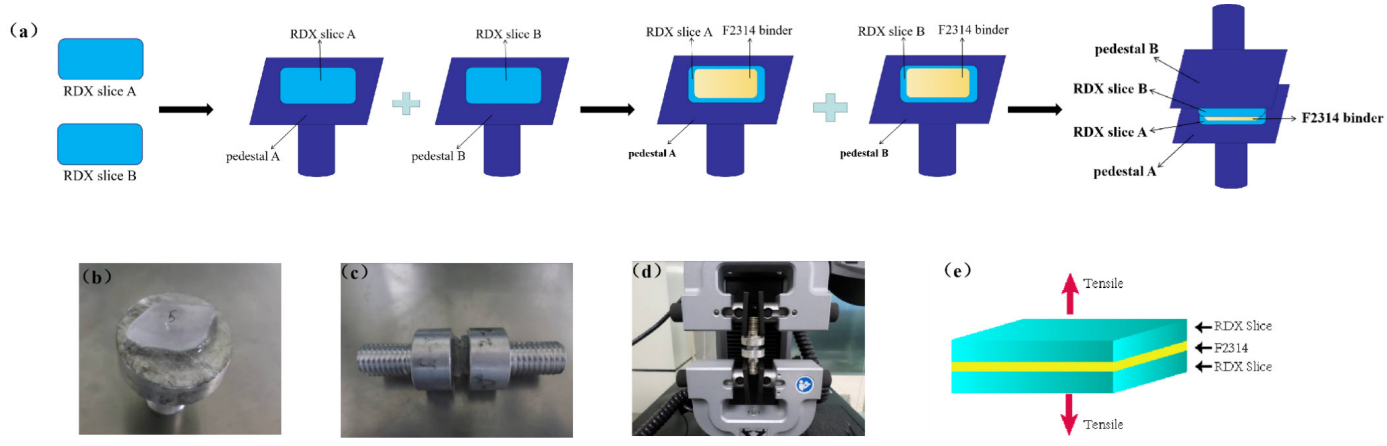


**Figure 2.** Schematic diagram and images of the adhesive strength measurement: schematic diagram for the preparation of the tensile test samples (a), images, of an RDX slice on the aluminum pedestal (b), of the RDX-F2314-RDX sandwich-like structure (c), in position in the material testing machine (d), and schematic diagram for the tensile test experiment (e)

# 3 Results and Discussion

## 3.1 RDX orientation and surface characteristics

XRD was used to orient each crystal slice as shown in Figure 3a. The peaks observed in the spectra obtained were almost straight lines, and there was almost no half-height width, indicating that the internal molecules of each crystal slice were arranged strictly according to the repeating unit. Compared with the full spectrum, single crystal faces of RDX (020), (210) and (002) were obtained. It can be seen from the surface roughness test results of the scanning probe microscope that the crystal surface was very smooth and the final root mean square (rsm) roughness of the surface was about 2.81 nm.

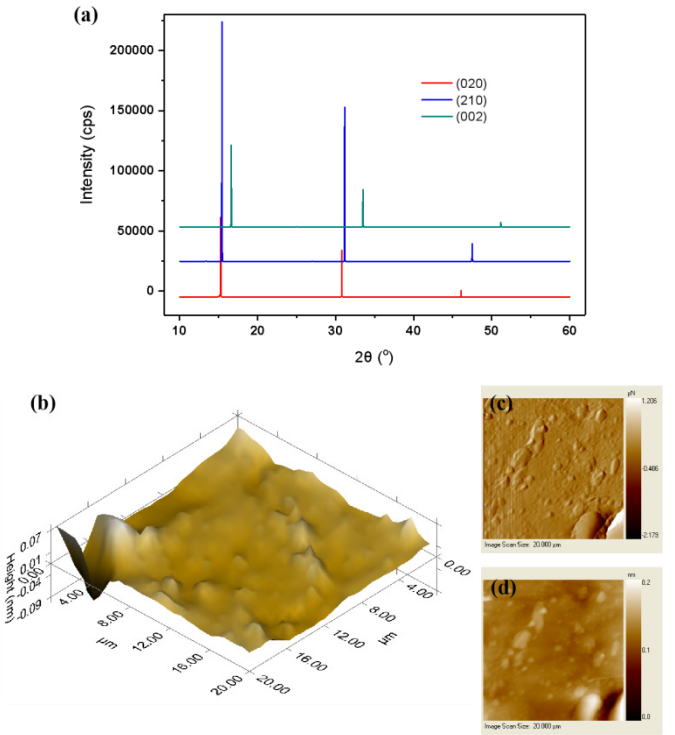


**Figure 3.** XRD spectrum of RDX slices (a), atomic force images for RDX(020) (b), and the scanning probe microscope images for RDX(210) (c) and RDX(002) (d)

### 3.2 Anisotropic interaction between RDX and F2314 from the contact angle test

Contact angle tests were carried out to study the interfacial interaction between RDX and F2314. Table 1 displays the contact angle of water and di-iodomethane on various crystal faces of RDX and of F2314.

**Table 1.** Contact angle of solution on RDX and F2314

| | RDX | | | F2314 |
|---|---|---|---|---|
| | (020) | (210) | (002) | |
| water | 68.79 | 75.57 | 86.37 | 98.24 |
| di-iodomethane | 35.71 | 36.20 | 40.46 | 60.30 |

The work of adhesion between RDX and F2314 can be calculated from Equation 1 [25].

$$W = \gamma_{\text{RDX}} + \gamma_{\text{F2314}} - \gamma_{\text{RDX-F2314}} \tag{1}$$

where $\gamma_{\text{RDX}}$ means the surface tension of RDX, $\gamma_{\text{F2314}}$ means the surface tension of F2314 and $\gamma_{\text{RDX-F2314}}$ means the interfacial tension between RDX and F2314.

The surface tension is essentially caused by the interactions between the molecules. The intermolecular interaction force ($\gamma$) can be divided into a polar force and a dispersive force (Equation 2).

$$\gamma = \gamma^p + \gamma^d \tag{2}$$

where $\gamma^d$ and $\gamma^p$ represent the non-polarity and polarity components, respectively. According to the Young equation, the surface tension and contact angle can be expressed as Equation 3.

$$\gamma_s - \gamma_{sl} = \gamma_l \cdot \cos\theta \tag{3}$$

where $\gamma_s$ is the surface tension of the solid material, $\gamma_{sl}$ is the interfacial tension between the solid and liquid, $\gamma_l$ is the surface tension of the liquid material, and $\theta$ is the contact angle. According to Fowkes theory, the relationship between the free energy of the interface between any two phases and the surface free energy and its components between the phases can be expressed as Equation 4.

$$\gamma_{sl} = [(\gamma_s^d)^{1/2} - (\gamma_l^d)^{1/2}]^2 + [(\gamma_s^p)^{1/2} - (\gamma_l^p)^{1/2}]^2 \tag{4}$$

Combining Equations 3 and 4 gives:

$$\gamma_l(1+\cos\theta) = 2(\gamma_s^d \gamma_l^d)^{1/2} + 2(\gamma_s^p \gamma_l^p)^{1/2} \quad (5)$$

Therefore, the surface energy, non-polarity and polarity forces of solid (RDX and F2314) could be obtained by Equations 1 and 5, in which the contact angles between liquid and solid could be measured, and are listed in Table 1. The surface tension ($\gamma_l$), non-polarity ($\gamma_l^d$) and polarity ($\gamma_l^p$) for two kinds of liquid (water and di-iodomethane in this work) were known parameters and are also listed in Table 2.

**Table 2** Physical properties of the solution (in $mN \cdot m^{-1}$)

| Solution | $\gamma_l$ | $\gamma l^d$ | $\gamma l^p$ |
|---|---|---|---|
| water | 72.75 | 22.10 | 50.65 |
| di-iodomethane | 50.80 | 48.50 | 2.30 |

From the data in Tables 1 and 2, the $\gamma^p$ and $\gamma^d$ of different RDX slices can be calculated by Equation 5. The surface energy can be obtained by Equation 1, and the results are shown in Figure 4. As shown in Figure 4(a), the $\gamma^d$ of RDX (020), (002) and (210) was 35.3, 37.4 and 36.8 $mN \cdot m^{-1}$, respectively, the $\gamma^p$ was 9.3, 2.0 and 5.8 $mN \cdot m^{-1}$, respectively, and the surface energy was 44.6, 39.4 and 42.6 $mN \cdot m^{-1}$, respectively. The surface energy of each crystal face was similar, and $\gamma^d$ accounted for the main part. The polar component was relatively small, but exhibited obvious anisotropic characteristics, which were closely related to the nitro group distribution on the crystal face. As shown in Figure 4(c), on the RDX(020) face, the nitro groups on the RDX molecules were all aligned on the plane of the crystal plane. On the RDX(002) face, two nitro groups in every four consecutive RDX molecules were arranged. The denser the nitro group distribution on the crystal face, the greater the contribution of the polar component to the surface energy.

As shown in Figure 4(b), the work of adhesion between the RDX face and F2314 was 70.0, 68.3 and 62.1 $mJ \cdot m^{-2}$, for RDX(020), (002) and (210), respectively. The work of adhesion was a combination of the polar component and the dispersion component, which also exhibited anisotropic characteristics for the various RDX crystal faces.

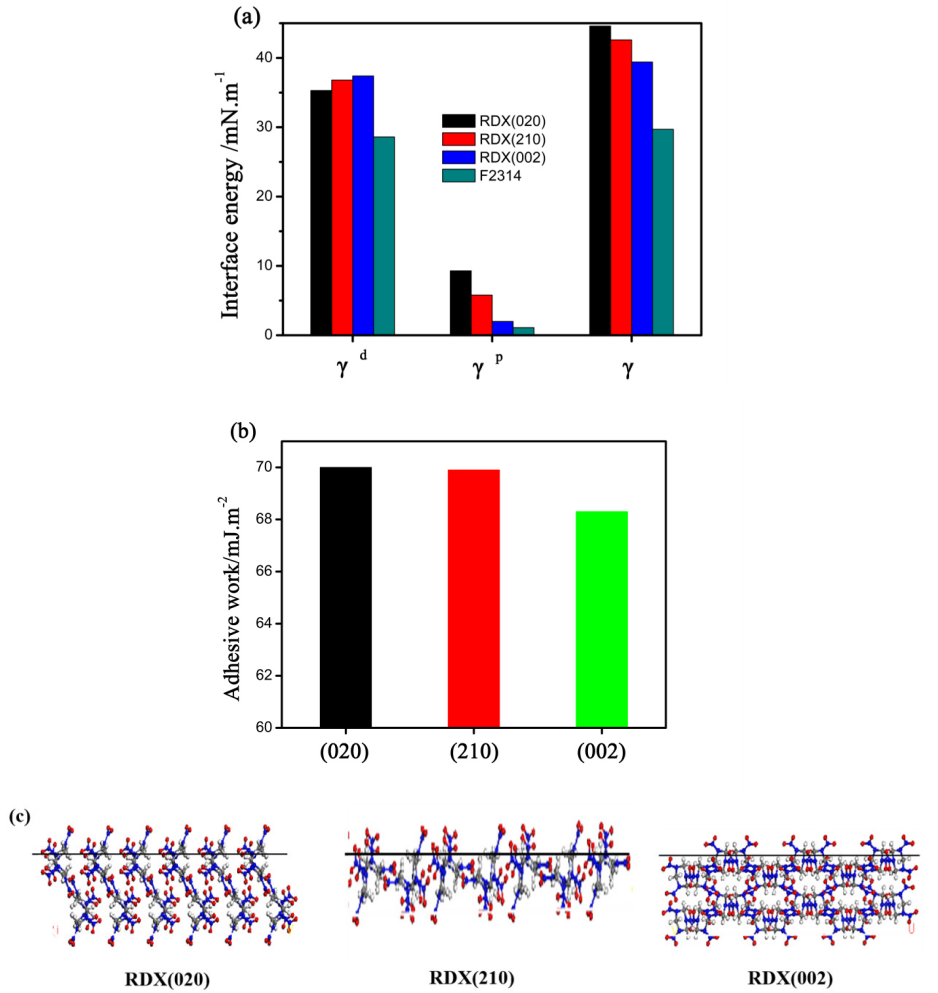


**Figure 4.** Surface energy of RDX slices and F2314 (a), the adhesive work between the RDX slices and F2314 (b), and the nitro group distribution on the different RDX faces (c)

In order to further understand the anisotropy of interfacial adhesion between F2314 and the various RDX surfaces, XPS was performed to obtain the level of each element. As presented in Table 3, after coating with F2314, the F element content on the (210), (020) and (002) faces was 25.50%, 25.44% and 28.94%, together with O atoms of 17.39%, 14.44%, and 12.85%, respectively. F2314 is a non-polar fluorinated polymer. The polar component of surface (002) was

smallest in the calculated result. In this case, the surface (002) possessed the maximum F and the least O atoms, probably due to better spreading of the F2314 binder on the RDX (002) surface. The non-polar fluorinated polymer was easier to spread on the surfaces with a lower polar component, which in turn caused the anisotropic spreading of F2314 on the various RDX surfaces.

**Table 3.** Surface element distribution data of RDX coated with F2314/%

| | Element | | | | |
|---|---|---|---|---|---|
| | C | O | N | F | Cl |
| RDX (020) | 37.24 | 14.44 | 16.62 | 25.44 | 5.74 |
| RDX (210) | 32.71 | 17.39 | 18.80 | 25.50 | 5.59 |
| RDX (002) | 41.49 | 12.85 | 10.3 | 28.94 | 5.69 |

### 3.3 Tensile tests for various RDX-F2314-RDX sandwich composites

Figure 5(a) shows the tensile stress-displacement curves for the different RDX-F2314-RDX sandwich composites. When the tensile stress was greater than the interfacial adhesion force, the interface began to debond and the stress curves peaked. This peak can be considered as the interfacial adhesive strength between the RDX crystal face and F2314. It can be seen that the interfacial adhesive strength between RDX(210), (020), (002) and F2314 was 1130 Pa, 796 Pa and 1042 Pa, respectively. It should be noted that the RDX (002) peak was determined at 1042 Pa, although the stress increased later, mainly because the stress had already dropped significantly at 1042 Pa, indicating that the interface had been debonded.

The work of adhesion for various RDX crystal faces and the F2314 binder was obtained by integrating the area under the displacement-strain curves, using the maximum tensile stress as the boundary. As can be seen from Figure 5(b), the work of adhesion measured by the direct tensile experiment between F2314 and RDX (210), (020), (002) were 51 ±10 mJ/m$^2$, 106 ±15 mJ/m$^2$ and 152 ±19 mJ/m$^2$, respectively. The differences between the work of adhesion results from the contact angle test and the tensile test was mainly attributed to the measurement method. Specifically, the tensile test was more sensitive to the anisotropy of the interfacial adhesive strength between RDX and F2314, compared with the results based on the contact angle test. Nevertheless, the values are of the same order of magnitude. Moreover, the results in this work demonstrated the anisotropy of the interfacial adhesion of F2314 on the various RDX crystal faces.

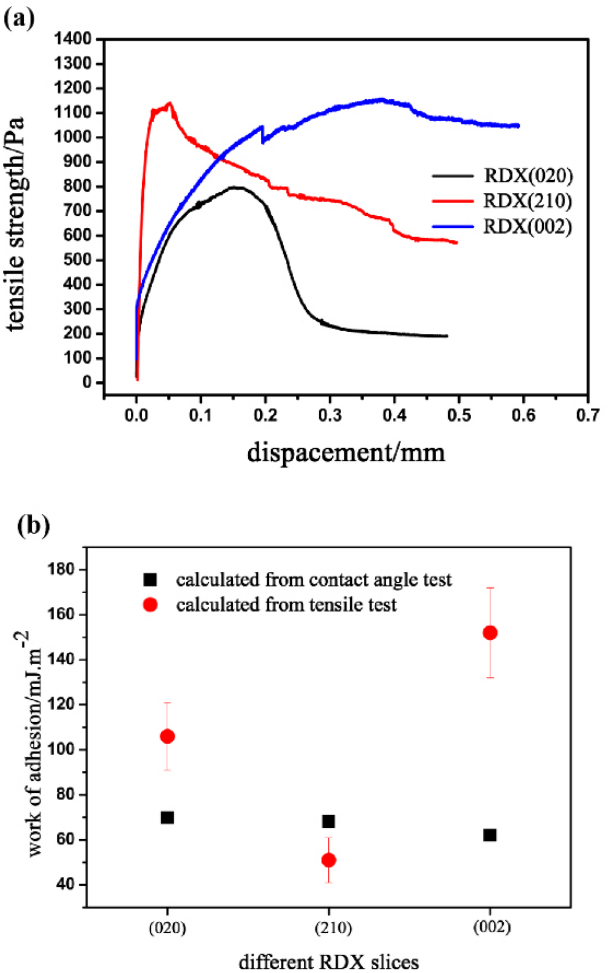


**Figure 5.** Tensile stress-displacement curves of the different RDX-F2314 sandwich composites (a), and the work of adhesion calculated from the tensile test and the contact angle test (b)

## 4 Conclusions

- In summary, this work demonstrated the anisotropic bonding between the F2314 binder and various RDX single crystal surfaces based on the systematic experimental and theoretical results.

- The work of adhesion measured by the direct tensile experiments between RDX (210), (020), (002) faces and the F2314 binder were 51 mJ/m$^2$, 106mJ/m$^2$ and 152 mJ/m$^2$, respectively. The polar component of the surface energy for the RDX surfaces exhibited obvious anisotropic characteristics, which in turn caused anisotropic spread of F2314 on the various RDX surfaces.
- The present results might provide a significant reference for tuning the crystallography to obtain particular surfaces for better performance of energetic materials.

## Acknowledgments

This work was supported by the National Natural Science Foundation of China (11872341, 21875232) and NSAF project (Grant No. U2030202).

## References

[1] Dobratz, B.M.; Crawford, P.C. *LLNL Explosives Handbook Properties of Chemical Explosives and Explosive Simulants.* US **1976**; UCRL-52997-Chg.2.
[2] Small IV, W.; Glascoe, E.A.; Overturf, G.E. Measurement of Moisture Outgassing of the Plastic-Bonded TATB Explosive LX-17. *Thermochim. Acta* **2012**, *545*: 90-95l DOI: 10.1016/j.tca.2012.06.033.
[3] Mirkarimi, P.B.; Moua, Y.; Pease, S.T.; Sain, J.D. Fracture Toughness and Crack Propagation in LX-17 and PBX 9502 Insensitive High Explosives. *Int. J. Solids Struct.* **2022**, *250*: 9-12; DOI: 10.1016/j.ijsolstr.2022.111721.
[4] Chen, P.; Huang, F.; Ding, Y. Microstructure, Deformation and Failure of Polymer Bonded Explosives. *J. Mater. Sci.* **2007**, *42*: 5272-5280; DOI 10.1007/s10853-006-0387-y.
[5] Yang, Z.; Lin, C.; Gong, F.; Zeng, C.; Zhang, J.; Huang, F. Effects of Crystal Quality and Morphology on the Mechanical Performance of LLM-105 Based PBXs. *Propellants Explos. Pyrotech.* **2019**, *44*(10): 1219-1225; DOI: 10.1002/prep.201900106.
[6] Li, Y.; Wu, P.; Hua, C.; Wang, J.; Huang, B.; Chen, J.; Qiao, Z.; Yang, G. Determination of the Mechanical and Thermal Properties, and Impact Sensitivity of Pressed HMX-based PBX. *Cent. Eur. J. Energ. Mater.* **2019**, *16*(2): 299-315; DOI: 10.22211/cejem/109717.
[7] Liu, J.-H.; Yang, Z.-J.; Liu, S.-J.; Zhang, J.-H.; Liu, Y.-G. Effects of Fluoropolymer Binders on the Mechanical Properties of TATB-based PBX. *Propellants Explos. Pyrotech.* **2018**, *43*(7): 664-670; DOI: 10.1002/prep.201700295.
[8] Liu, R.; Han, Y.; Li, M.; Jiang, Z.; He, S. Shock Ignition and Growth of HMX-based PBXs under Different Temperature Conditions. *Cent. Eur. J. Energ. Mater.* **2019**, *16*(1): 21-32; DOI: 10.22211/cejem/104390.

[9] Hobbs, M.L.; Kaneshige, M.J. Ignition Experiments and Models of a Plastic Bonded Explosive (PBX 9502). *J. Chem. Phys.* **2014**; *140*, paper 124203; DOI: 10.1063/1.4869351.

[10] Li, T.; Hua, C.; Li, Q. Shock Sensitivity of Pressed RDX-based Plastic Bonded Explosives Under Short-duration and High-Pressure Impact Tests. *Propellants Explos. Pyrotech.* **2013**, 38: 770-774.

[11] He, G.; Yang, Z.; Pan, L.; Zhang, J.; Liu, S.; Yan, Q.-L. Bioinspired Interfacial Reinforcement of Polymer Based Energetic Composites with a High Loading of Solid Explosive Crystals. *J. Mater. Chem. A* **2017**, *5*(26): 13499-13510; DOI: 10.1039/C7TA03424E.

[12] Gholamian, F.; Ansari, M.; Abdullah, M.; Bataghva, F.; Ghariban-Lavasani S. Intermolecular Interaction of a Neutral Polymeric Bonding Agent Containing N-Vinylpyrrolidone Units with Ammonium Perchlorate and Keto-RDX. *Chin. J. Polym. Sci.* **2013**, *31*(10): 1372-1381; DOI: 10.1007/s10118-013-1327-3.

[13] Lin, C.; Huang, B.; Gong, F.; Yang, Z.; Liu, J.; Zhang, J.; Zeng, C.; Li, Y.; Li, J.; Guo, S. Core@Double-Shell Structured Energetic Composites with Reduced Sensitivity and Enhanced Mechanical Properties. *ACS Appl. Mater. Interfaces* **2019**, *11*(33): 30341-30351; DOI: 10.1021/acsami.9b10506.

[14] Zhao, Y.; Xie, W.; Qi, X.; Liu, Y.; Tang, Q.; Song, K.; Zhang, W. Comparison of the Interfacial Bonding Interaction Between GAP Matrix and Ionic/non-Ionic Explosive: Computation Simulation and Experimental Study. *Appl. Surf. Sci.* **2019**, *497*(1): 143813; DOI: 10.1016/j.apsusc.2019.143813.

[15] Jaidann, M.; Lussier, L.-S.; Bouamoul, A.; Abou-Rachid, H.; Brisson, J. Effects of Interface Interactions on Mechanical Properties in RDX-Based PBXs HTPB-DOA: Molecular Dynamics Simulations. *Proc. 9th Int. Conf. Computational Science – ICCS 2009,* Part II, (Allen, G.; Nabrzyski, J.; Seidel, E.; van Albada, G.D.; Dongarra, J.; Sloot, P.M.A., Eds.) Springer-Verlag, Berlin/Heidelberg/New York, **2009**, 131-140; ISBN-13: 978-3-642-01972-2.

[16] Yeager, J.D.; Dattelbaum, A.M.; Orler, E.B.; Baht, D.F.; Dattelbaum, D.M. Adhesive Properties of Some Fluoropolymer Binders with the Insensitive Explosive 1,3,5-Triamino-2,4,6-trinitrobenzene (TATB). *J. Colloid Interface Sci.* **2010**, *352*(2): 535-541; DOI: 10.1016/j.jcis.2010.08.063.

[17] Du, M.-N.; Luo, Y. Effect of Particle Size and Surface Free Energy of RDX on the Mechanical Properties of HTPB Propellant. *Chin. J. Energ. Mater.* **2008**, *16*(4): 441-445.

[18] Wang, D.; Shu, Y.-J.; Li, M.; Chen, T.-N.; Kang, B.; Song, M.-X. Fracture Toughness of RDX and HMX Single-crystal by Indentation. (in Chinese) *Chin. J. Explos. Propell.* **2011**, *34*(1): 28-31.

[19] Li, M.; Tan, W.-J.; Kang, B.; Xy, R.-J.; Tang, W. The Elastic Modulus of β-HMX Crystals Determined by Nanoindentation. *Propellants Explos. Pyrotech.* **2010**, *35*(4): 379-383; DOI: 10.1002/prep.201000018.

[20] Zhou, X.; Xu, R.; Huang, M. Characterization of Dislocation in RDX Single Crystal by Rocking Curve. *Proc. 43rd Int. Annu. Conf. ICT*, Fraunhofer, Germany, **2012**.

[21] Williamson, D.M.; Palmer, S.J.P.; Proud, W.G. Thermodynamic Work of Adhesion Between HMX and a UK PBX Binder System. *Shock Compression of Condensed Matter* **2009**: 478-481.
[22] Li, H.; Zhou, X.; Xu, R. Growth and Machining of RDX Single Crystal, *Chin. J. Energ. Mater.* **2011**, *19*(6): 745-746.
[23] Zhou, X.; Li, H.; Liu, J. Precision Machining of RDX Single Crystal, *Chin. J. Energ. Mater.* **2013**, *21*(5): 693-695.
[24] *Paints and Varnishes – Pull-off Test for Adhesion.* Standard GB-T5210-2006, **2006**.
[25] He, G.; Liu, J.; Gong, F. Bioinspired Mechanical and Thermal Conductivity Reinforcement of Highly Explosive-filled Polymer Composites. *Compos. Part A.* **2018**, 107: 1-9.

Received: May 5, 2021
Revised: December 22, 2022
First published online: December 23, 2022